

Collaborative Exploration of Mineral Resources and Renewable Energy Using Remote Sensing Data Intelligent Processing Technology

Hongqi Ren*

Chongqi Jiaotong University, Chongqing 400030, Chongqing, China

*Correspondence author's email: 15102310551@163.com

Abstract. Traditional collaborative exploration methods for mineral resources and renewable energy often rely on manual experience and simplified models, resulting in low efficiency and precision in mineral resource and renewable energy exploration, as well as apparent deficiencies in multi-source data fusion and environmental impact assessment. In response to this situation, this paper combines the intelligent processing technologies of remote sensing data, such as convolutional neural networks (CNNs) and long short-term memory (LSTM) networks, to improve the spatial recognition and time series analysis capabilities of mineral resources and renewable energy exploration, realize the precise identification of resources, spatiotemporal change monitoring, and collaborative development, and optimize resource allocation and environmental impact assessment. During the research process, this study first uses multi-source fusion technology of remote sensing data to preprocess optical images, radar data, and geological data to ensure the comprehensiveness and diversity of the data. Then, CNN is used to extract spatial features. LSTM is used to analyze temporal information to construct a multimodal deep learning framework for the collaborative exploration of mineral resources and renewable energy. Subsequently, the effectiveness of the proposed method is verified through experimental design. The experimental results indicate that the joint model constructed in this paper performs well in exploration precision, computational efficiency, resource consumption, and model robustness. When exploring 1,000 remote sensing images, the proposed model has an accuracy of 85.6% and a recall of 82.3%, demonstrating high exploration precision. When processing data sets of different sizes, the processing efficiency of the model in this paper is 2.19 images/second, 2.15 images/second, and 2.09 images/second, respectively, which performs better than most control groups. Comprehensive analysis shows that the model constructed in this paper exhibits excellent performance in many aspects and can provide adequate support for the practical application of remote sensing images.

Key words. Remote sensing data, Intelligent processing

technology, Mineral resources, Renewable energy, Collaborative exploration

1. Introduction

As global energy transformation and environmental protection become the focus of international attention, the coordinated exploration of mineral resources and renewable energy has gradually become an important way to cope with the energy crisis, reduce carbon emissions, and achieve sustainable development [1-3]. Due to the growing demand for renewable energy in various countries and the necessity of continuous mining of mineral resources, the efficient joint exploration and development of mineral resources and renewable energy has become an important research topic in the current energy field [4,5]. The exploration research of mineral resources and renewable energy should become an important part of the research on spatial distribution, temporal changes and environmental impact assessment [6-8]. Traditional exploration methods mainly rely on manual experience, simplified models and single data sources [9,10]. Their exploration efficiency and accuracy are low, especially in multi-source data fusion and environmental impact assessment. Specifically, traditional methods cannot effectively integrate multi-source information such as optical images, radar data and geological data, resulting in insufficient accuracy of resource identification and timeliness of spatiotemporal change monitoring. In addition, traditional methods lack systematicity in environmental impact assessment and cannot fully predict the long-term impact of resource development on the ecological environment, thus affecting the balance between resource development and environmental protection.

To overcome these challenges, this paper proposes an improved method based on remote sensing data intelligent processing technology, which combines convolutional neural networks (CNN) and long short-term memory networks (LSTM) to achieve accurate identification and spatiotemporal change monitoring of mineral resources and renewable energy

collaborative exploration. Compared with traditional methods, this method has made significant improvements in multi-source data fusion and environmental impact assessment. First, in terms of multi-source data fusion, CNN can extract high-precision spatial features from remote sensing images, while LSTM can capture dynamic change information in time series data, thereby achieving a comprehensive interpretation and dynamic monitoring of resource distribution. This combination not only improves the recognition accuracy of the spatiotemporal distribution characteristics of mineral resources and renewable energy, but also enhances the adaptability to complex terrain and climatic conditions. Secondly, in terms of environmental impact assessment, this method can analyze the dynamic trend of resource development through the time series modeling capability of LSTM, while the spatial feature extraction capability of CNN can monitor the spatial changes of mining areas and renewable energy areas in real time. This spatiotemporal analysis capability provides a more comprehensive basis for environmental impact assessment, helps to reduce the negative environmental impacts in collaborative exploration, and ensures a balance between resource development and environmental protection.

In addition, this study also aims to optimize resource allocation and improve the accuracy of environmental impact assessment, especially to reduce the negative environmental impact in collaborative exploration and ensure the balance between resource development and environmental protection. These research results provide a new intelligent method for the exploration of mineral resources and renewable energy, and a new technical path for promoting global energy transformation and achieving sustainable development goals, thus providing all-round support for the effective development of mineral resources and the joint utilization of renewable energy.

Main contributions: (1) An effective remote sensing image exploration model is established. From the experimental results, the model has high exploration precision and short processing time on data sets of different scales, which improves the effectiveness of remote sensing image exploration. (2) The model's resource consumption and computational efficiency are evaluated. To promote the application of the model in large-scale remote sensing image analysis, this paper rigorously evaluates the model's computational efficiency and resource consumption at different data scales. (3) The robustness of the model is tested. Noise interference experiments verify that the proposed model still maintains high exploration precision and recall in a high-noise environment, showing good robustness.

2. Literature Review

As an important exploration method, remote sensing technology has been widely applied to the fields of mineral resources, renewable energy, etc. [11,12]. As the

remote sensing platform technology advances continuously, the types of remote sensing data and spatial resolution have been continuously improved, and significant results have been achieved in resource distribution analysis, identification, exploration, and monitoring [13-15]. By integrating multi-source remote sensing information represented by high-resolution images, optical images, and radar data, it is possible to more accurately interpret the spatial distribution characteristics of mineral resources, analyze resource evolution, and conduct dynamic monitoring. In renewable energy, remote sensing data plays an indispensable role in resource potential assessment of solar energy, wind energy, and other resources, environmental monitoring, and other aspects, providing reliable data support for sustainable development [16]. However, although remote sensing technology has realized remarkable results in resource exploration, it still faces challenges in multi-source data fusion, spatiotemporal feature extraction, and environmental impact assessment [17-19]. In recent years, intelligent processing technology, especially deep learning technology, has had great development potential in the intelligent analysis of remote sensing data. CNN performs well in image feature extraction and can efficiently extract spatial features in remote sensing images and improve the precision of resource identification [20]. LSTM has unique advantages in time series data analysis and can capture dynamic information about data changes over time. It is particularly suitable for temporal and spatial trend analysis of mineral resources and renewable energy [21]. Although some progress has been made in the application of deep learning technology in remote sensing data processing, it still faces many challenges in large-scale data processing, algorithm optimization, and model generalization [22-24]. In addition, the combination of deep learning and traditional remote sensing technology remains a hot and difficult research topic on improving its applicability in complex environments. The collaborative exploration of mineral resources and renewable energy has been a research direction that has received much attention recently, which can help promote energy transformation and realize sustainable development [25,26]. Traditional mineral resource exploration methods are mainly based on manual experience and simplified models, and their results are often inefficient and lack systematicity in environmental impact assessment and resource allocation [27,28]. With the rapid development of intelligent technologies, collaborative exploration methods based on deep learning and remote sensing data have gradually emerged in recent years and become a new trend [29]. Dong L and Wei J T both pointed out in their 2023 study that most existing research focuses on the exploration and development of a single resource, and there is little systematic discussion on the coordinated development of mineral resources and renewable energy [30,31]. Therefore, using remote sensing data and intelligent processing technology to improve the efficiency and precision of the collaborative exploration of mineral resources and renewable energy is the future development direction. This study aims to fill the gap in this area and optimize and apply the collaborative

exploration method of mineral resources and renewable energy using remote sensing data intelligent processing technology based on CNN and LSTM.

3. Implementation of Collaborative Exploration Method for Mineral Resources and Renewable Energy Based on CNN and LSTM

In this paper, CNN and LSTM are selected as the main models because CNN is good at extracting spatial features from remote sensing images, while LSTM can effectively capture dynamic changes in time series data. This combination not only meets the dual needs of spatial identification and temporal analysis in the coordinated exploration of mineral resources and renewable energy, but also improves the accuracy of resource identification and the timeliness of spatiotemporal change monitoring through multi-source data fusion.

A. Remote Sensing Data Acquisition and Preprocessing

1) Data Collection

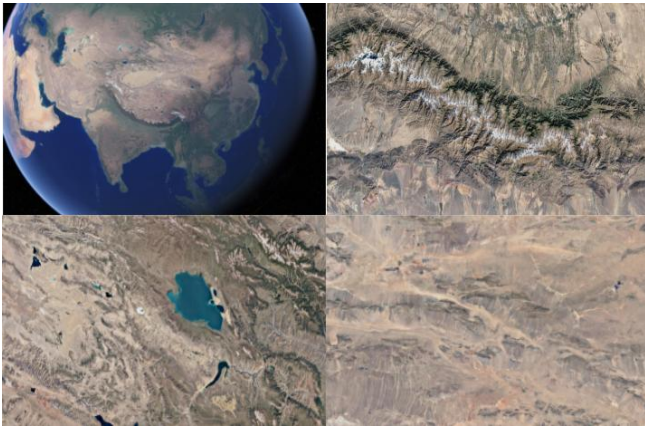


Figure 1. Some examples of remote sensing images.

The data collection work for this study provides key support for the collaborative exploration of mineral resources and renewable energy. The remote sensing data comes from multiple satellite platforms and aerial remote sensing systems, covering specific geographical areas, including mountainous areas rich in mineral resources and coastal areas with great potential for renewable energy. The optical image data mainly comes from the Landsat 8 satellite of NASA (National Aeronautics and Space Administration) in the United States, covering remote sensing images from 2018 to 2024. The data resolution is 30 meters, which is suitable for surface resource identification and spatial distribution analysis, especially for monitoring mineral resources in plateaus and mountainous areas. The radar data comes from the Sentinel-1 satellite of the European Union's Copernicus program, which acquires synthetic aperture radar (SAR) data from 2019 to 2022. It has a high temporal and spatial resolution and can penetrate clouds and

atmospheric interference, which is suitable for resource detection in complex terrain and climatic conditions and is mainly used for resource detection in mountainous areas and coastal wetlands. Figure 1 presents some images.

High-resolution drone image data is acquired by the research team in specific mineral exploration areas in 2023. The data resolution is 10cm, which is suitable for high-precision local exploration and is mainly used for local resource exploration in urban areas and mining areas.

In addition, ground observation data also provides supplementary support for remote sensing data. Meteorological data, such as temperature, humidity, and wind speed, and information, such as soil type and vegetation cover, are collected in the selected mining area and renewable energy potential assessment area, covering an area of about 5,000 square kilometers. The amount of remote sensing image data accumulates to more than 3,000 pieces, covering various time periods, climate conditions, and geographical areas, providing rich data support for subsequent analysis and model training.

2) Data Preprocessing

The remote sensing image data collected in this study are thoroughly preprocessed to ensure that the data quality meets the needs of further analysis. First, geometric correction is performed to address the geometric distortion in the remote sensing image. The image is precisely aligned with the geographic coordinate system by matching with the ground control points. This process solves the spatial inconsistency problem caused by sensor bias, shooting angle changes, or terrain factors, ensuring the effective fusion of multi-temporal and multi-source data, which is especially important when conducting temporal and spatial comparative analysis. In the geometric correction process, the following formulas are used to adjust the geometric distortion of the image:

$$x' = a_1x + a_2y + a_3 \quad (1)$$

$$y' = a_4x + a_5y + a_6 \quad (2)$$

Among them, x' and y' represent the coordinates after correction. x and y represent the coordinates in the original image. a_1 , a_2 , a_3 , a_4 , a_5 , and a_6 are the transformation parameters obtained by least squares fitting.

Considering that different data sources have significant differences in spatial resolution, spectral response characteristics, observation angles, and sensor configurations, this paper introduces a series of multi-source data standardization and differential processing strategies in the data preprocessing stage to

improve the quality of remote sensing data fusion and the consistency of modeling foundation.

First, in the spatial dimension, in order to address the problem of inconsistent resolution, a method based on bicubic interpolation is used to resample all images to a uniform spatial resolution (set to 10m in this paper) to ensure a consistent spatial scale for subsequent feature extraction. For geometric distortion, the remote sensing data of each phase are aligned to a unified geographic coordinate frame through an orthogonal geometric correction method based on control point matching, and the registration error is controlled within 0.5 pixels.

Second, in the spectral dimension, in order to address the differences in band settings between different sensors, this paper handles spectral differences through the strategies of band matching and feature mapping. Specifically, for the C-band radar data of Sentinel-1 and the optical band data of Landsat, principal component analysis (PCA) is used to reduce the dimensionality of the spectral information and construct a unified feature space. On this basis, the spectral correlation between different data sources is quantified by mutual information to screen out fusion bands with complementary information. For example, Band 5 of Landsat and the VV polarization intensity of Sentinel-1 show a strong correlation in vegetation monitoring, and are used as joint features for subsequent modeling.

In the time dimension, linear interpolation and Gaussian weighted smoothing are used to fill and denoise the time series to reduce modeling errors caused by inconsistent observation intervals or outliers.

Based on the above preprocessing, radiation normalization and atmospheric correction are further performed on the image data. In order to reduce the deviation caused by changes in meteorological conditions, sensor response differences or changes in illumination, this paper uses the 6S (Second Simulation of Satellite Signal in the Solar Spectrum) radiation transfer model based on the physical model for atmospheric correction. This model can accurately simulate the propagation process of solar radiation in the atmosphere, taking into account parameters such as atmospheric thickness, aerosol type, water vapor content and ozone concentration, and can better reflect the real physical process than statistical regression or PCA methods. The corrected surface reflectivity ρ is expressed by the following formula:

$$\rho = \frac{\pi \cdot (L_{\text{sat}} - L_{\text{path}})}{T_s \cdot T_v \cdot E_{\text{sun}} \cdot \cos \theta} \quad (3)$$

Among them, L_{sat} is the radiation brightness received by the satellite, L_{path} is the path radiation (i.e., atmospheric scattering contribution), T_s and T_v are the atmospheric transmittances from the sun to the surface and from the surface to the sensor, respectively, E_{sun} is the solar irradiance, and θ is the solar zenith angle. Compared with the atmospheric correction methods based on PCA and statistical regression, the radiation transfer model can more accurately simulate the influence of the atmosphere on spectral information, thereby more accurately restoring the surface radiation value. The PCA-based method mainly focuses on the principal component analysis of the data, which may not fully consider the physical characteristics of the atmosphere. The statistical regression-based method requires a large amount of training data and may be limited by model assumptions. The radiation transfer model can more accurately describe the influence of the atmosphere on spectral information through physical modeling, and is suitable for complex atmospheric environments and scenes with high precision requirements.

In response to noise interference in the image, this study uses Gaussian filtering technology to remove sensor noise and environmental noise in the data. The denoising process is as follows:

$$I_{\text{denoised}}(x, y) = \frac{1}{N} \sum_{i=-k}^k \sum_{j=-k}^k I(x+i, y+j) \quad (4)$$

$I_{\text{denoised}}(x, y)$ represents the pixel value of the denoised image. $I(x, y)$ represents the pixel value of the original image. k represents the size of the filter window. N represents the number of pixels in the window. Compared with other denoising methods, such as median filtering and wavelet denoising, Gaussian filtering can better retain image details while removing noise. Median filtering is effective in removing salt and pepper noise, but may lose image details when processing Gaussian noise. Wavelet denoising can better retain image details, but the computational complexity is high and it is sensitive to parameter selection. Gaussian filtering can better retain the main features of the image while removing noise through smoothing, and is suitable for preprocessing of remote sensing images.

B. CNN for Spatial Feature Extraction

1) Overview of CNN Model

CNN is a popular deep learning model used to solve computer vision problems, especially feature extraction and image classification. Figure 2 presents its structure:

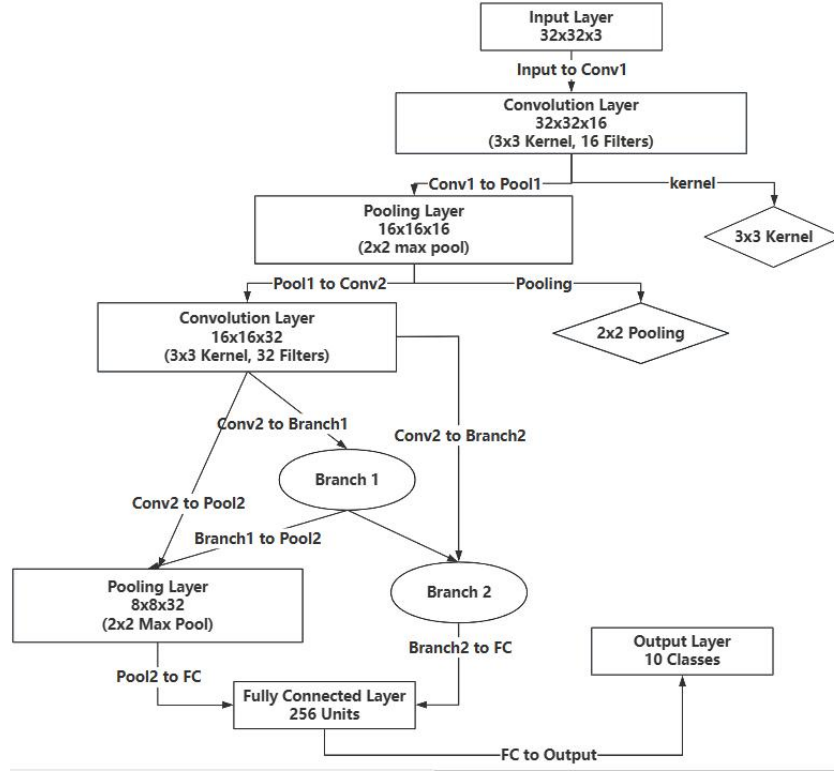


Figure 2. CNN structure.

The basic architecture of CNN consists of several layers, namely convolutional layers, pooling layers, and fully connected layers. Each layer has a different purpose by gradually extracting and modifying the features of the input data, allowing the model to automatically obtain valuable information from the image. The key component of CNN is the convolutional layer, which extracts local area features by sliding the convolution kernel on the image. Formula (5) can be used to represent the convolution operation:

$$(I * K)(i, j) = \sum_m \sum_n I(i + m, j + n) K(m, n) \quad (5)$$

Low-level features in images can be identified through the convolution method, such as edges, textures, and shapes. By stacking multiple convolutional layers, it is able to capture abstract features at a higher level. Through the downsampling process, the pooling layer reduces the dimension of the feature map retrieved by the convolutional layer, thereby minimizing the amount of computation while improving feature elasticity. Max pooling and average pooling are common pooling operations. The following is the expression of the max pooling operation:

$$P(i, j) = \max_{(m, n) \in R} I(i + m, j + n) \quad (6)$$

Among them, $P(i, j)$ is the output after pooling, and R is the area of the pooling window. Pooling can effectively remove irrelevant noise while retaining the

essential information of the features. After passing through multiple convolutional layers and pooling layers, the feature map is transmitted to the fully connected layer at the end of the network. The fully connected layer couples the output layer with high-level abstract features to complete image classification or regression operations. The fully connected layer helps the model make final predictions by transferring the spatial features extracted by the convolutional layer to the final output category or value [32].

2) Spatial Feature Extraction

In remote sensing image analysis, spatial feature extraction is the core link to understanding the distribution of geographical areas and target objects. CNN can effectively identify complex terrain, mineral resource distribution, and renewable energy potential areas by extracting spatial features from images layer by layer. The convolutional layer of CNN first focuses on the extraction of low-level features, such as edges, corner points, textures, and basic shapes. These features are the most direct spatial information in the image, especially in remote sensing images of mineral resource distribution. For example, the boundaries of mining areas usually appear as strong grayscale or color changes. The convolution operation can effectively capture these edge features and then calibrate the location of the mining area. The convolution kernel performs local convolution on the image through a sliding window, thereby extracting contrast differences in the image and helping to analyze the boundaries of mining areas and their spatial distribution characteristics.

As the network level deepens, CNN further extracts more abstract spatial features. Deep convolutional layers can identify more complex geographical features, such as the distribution pattern of mining areas, mountains, hills, etc. At this time, the convolution kernel not only focuses on low-level edges or textures but also captures more complex shape and structure information. Features such as terrain ups and downs and river distribution are usually manifested as unique textures, colors, or shapes in images. Deep convolutional layers can precisely identify these complex features. This process can be expressed by the formula:

$$F_l(i, j) = \sum_{k=1}^K I_{l-1}(i+m, j+n) \cdot W_l(k) \quad (7)$$

$F_l(i, j)$ is the feature extracted by the l -th convolutional layer. $W_l(k)$ is the convolution kernel of the l -th layer. I_{l-1} is the feature map of the previous layer. This process enables deep feature maps to help the network understand more complex spatial patterns in the image.

After feature extraction, the pooling layer further simplifies the image representation by reducing the dimension, enhancing the model's robustness to complex terrain features. Especially in remote sensing images with complex climate and geographical conditions, the pooling operation helps to remove redundant information and retain key features. Pooling operations commonly use maximum pooling and average pooling, among which maximum pooling retains the most significant features in the local area, which is particularly important for extracting spatial features such as mining area boundaries and terrain changes.

In addition, CNN has the ability to extract multi-scale features and can identify spatial features at multiple

scales. Features of different regions in remote sensing images may be more significant at different scales. CNN extracts features from various scales through multi-layer convolution operations. It can identify large-scale terrain features and precisely detect subtle changes in local areas. For large-scale terrain such as mountains and hills, CNN can capture its overall shape through deep convolution. For detailed features such as roads and rivers, CNN extracts more detailed local changes through shallower convolution. This multi-scale learning process can be expressed by Formula (8):

$$F_{\text{scale}} = \sum_{l=1}^L (I * K_l) \quad (8)$$

Among them, F_{scale} represents multi-scale features, and L represents the total number of convolutional layers. Through this mechanism, CNN can fully extract rich spatial information from images, thereby providing precise recognition of complex spatial distribution features in remote sensing images.

C. LSTM for Time Series Data Analysis

1) Overview of LSTM Networks

LSTM is a special type of recurrent neural network (RNN). Its core advantage is that it effectively overcomes the gradient vanishing and gradient exploding problems of traditional RNN when dealing with long-term dependency problems. Traditional RNN finds it difficult to effectively transmit long-term dependency information when the time step increases, resulting in poor performance when facing longer time-dependent tasks. LSTM can retain long-term information and suppress the flow of irrelevant information through its unique network structure, significantly improving the ability to model long-term dependency relationships. Figure 3 presents the LSTM network structure:

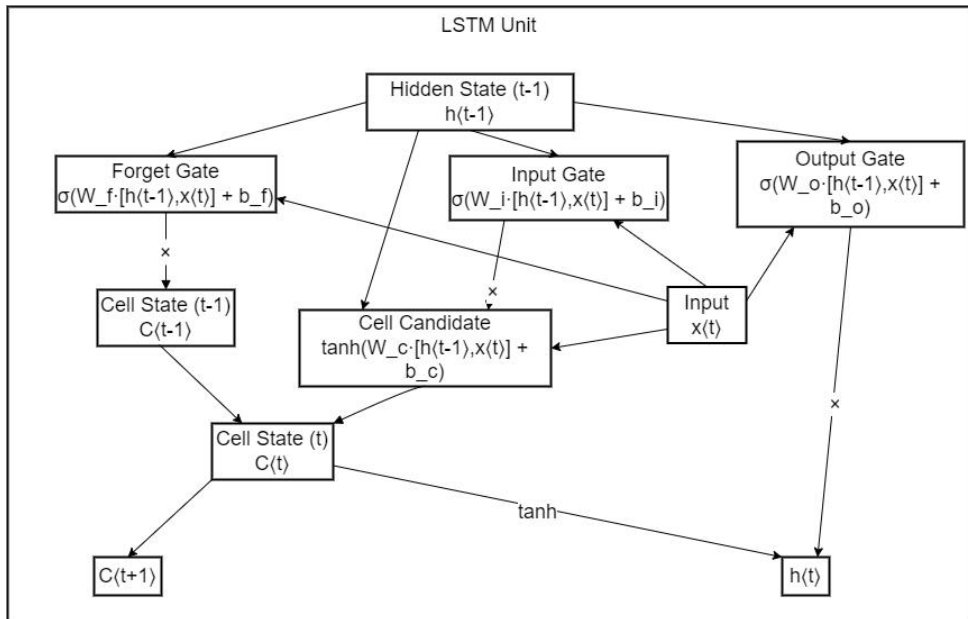


Figure 3. LSTM network structure.

The input gate, forget gate, and output gate are the three main gating mechanisms that make up the LSTM network. These gating methods improve the network's ability to identify long-term dependencies in time series data by carefully regulating the flow of information and deciding which data should be saved, modified, or deleted. Specifically, which new data is written to the memory cell is controlled by the input gate. To determine which information should be retained in the memory cell and measure the relevance of the incoming information, it performs a weighted sum of the current input and the network output at the previous moment to generate a number between 0 and 1. The following is the computation formula:

$$i_t = \sigma(W_i \cdot [h_{t-1}, x_t] + b_i) \quad (9)$$

Among them, i_t is the output of the input gate. The Sigmoid activation function is represented as σ . The weight and bias of the input gate are represented as W_i and b_i , respectively. The hidden state at the previous moment is represented as h_{t-1} . The input at the current moment is x_t . Which data is removed from the memory cell is determined by the forget gate. Its computation formula is:

$$f_t = \sigma(W_f \cdot [h_{t-1}, x_t] + b_f) \quad (10)$$

The forget gate filters out irrelevant or outdated information based on the current input and the output of the previous moment, maximizes the content of the memory cell, and generates a value between 0 and 1, indicating the proportion of information retained. The output gate is responsible for taking the output data of the current moment out of the memory cell and sending it to the subsequent layers of the network. Its computation formula is:

$$o_t = \sigma(W_o \cdot [h_{t-1}, x_t] + b_o) \quad (11)$$

It determines the impact of the memory content at the current moment on subsequent computations and predictions. By dynamically adjusting the output gate, LSTM can flexibly control the flow of information at different time steps, thereby improving the model's adaptability.

2) Time Series Data Analysis

Given its distinctive network architecture, LSTM primarily serves to identify extended patterns within sequential data observations, particularly in environmental monitoring applications. Through specialized control components, LSTM manages temporal data streams by selectively retaining or discarding information – that is to say, it learns complex

temporal relationships through adaptive memory systems.

Specifically, the framework utilizes three regulatory mechanisms: input regulators determine how incoming observations update internal memory storage, elimination filters decide which historical patterns become less relevant over time, and output controllers shape final predictions based on accumulated knowledge. To put it simply, these components work together to maintain useful historical patterns while filtering outdated details that might reduce predictive accuracy.

In environmental monitoring scenarios, LSTM identifies multi-year trends from accumulated datasets, such as seasonal patterns in mineral availability, decade-long climate variations, and evolving extraction processes across mining operations. By progressively updating its memory storage, the system detects cyclical phenomena and applies these insights for forecasting future resource conditions. For instance, it might predict mineral depletion timelines through historical seasonal fluctuations or estimate extraction timelines based on cumulative usage trends observed in past decades.

Similarly for sustainable energy assessments, LSTM recognizes connections between weather pattern shifts and energy output fluctuations. Through analysis of historical climate records, it forecasts production variations in weather-dependent energy sectors like solar farms or wind turbine arrays. By learning repeating cycles within observational data, the technology supports energy infrastructure planning through predictive models of supply-demand imbalances – an approach that helps optimize resource allocation despite inherent environmental uncertainties.

D. Multi-source Data Fusion and Collaborative Analysis

1) Multi-source Data Fusion

A key technical step in this study is multi-source data fusion, which attempts to effectively combine multiple forms of remote sensing data, including optical images, radar data, geological data, etc., to extract more detailed information and provide a detailed basis for resource development. Since remote sensing data have different spatial resolutions, temporal resolutions, and band characteristics, efficiently utilizing the advantages of various types of data for precise fusion has become the key to improving resource exploration precision. Based on the preprocessed data in the previous paper, multi-source data fusion technology is adopted to integrate these heterogeneous data into a unified information platform, thereby further enhancing the comprehensive application value of the data. Figure 4 presents the specific fusion process:

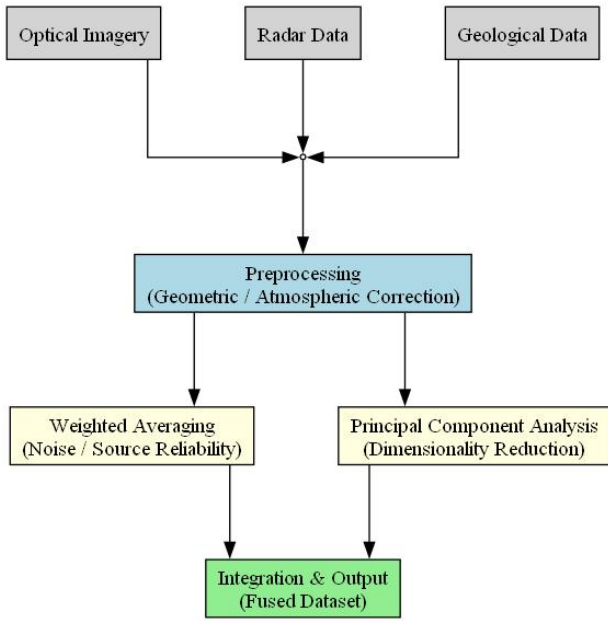


Figure 4. Multi-source data fusion process.

This study uses principal component analysis (PCA) and weighted average method for data fusion, aiming to effectively deal with noise and inconsistency in multi-source remote sensing data. In the process of multi-source remote sensing data fusion, there may be quality differences, noise interference and inconsistency among the data sources, especially in the case of different spatial resolutions, observation times and sensor types. In order to meet these challenges, the data sources are first processed by the weighted average method, and different weights are assigned to different data sources. This method weights each data source according to its accuracy and reliability, effectively reducing the impact of noise and errors. The weighted average formula is as follows:

$$D_{\text{fused}} = \sum_{i=1}^n w_i D_i \quad (12)$$

Among them, D_{fused} is the fused data, D_i is the i -th data source, w_i is the weight of the i -th data source, and n is the total number of data sources. In this way, the advantages of each data source can be maximized in the fusion process, and the impact of low-quality data sources can be reduced, which is especially suitable for situations where there are differences in the quality and importance of data sources.

In addition, in order to further reduce the redundant information and noise in multi-source data, this study also uses PCA for dimensionality reduction. PCA removes redundant information and reduces noise by mapping high-dimensional data to low-dimensional space, thereby enhancing the validity of the data. Through orthogonal transformation, PCA can extract the main features in multi-source data and further improve the accuracy of subsequent analysis. Its mathematical

expression is:

$$Z = XW \quad (13)$$

Among them, X represents the raw data matrix. W represents the transformation matrix composed of eigenvectors. Z represents the data after dimensionality reduction. Through PCA, multi-source data can be projected onto new coordinate axes, and the main features of each data source can be extracted, further improving the validity of the data and the precision of analysis.

2) Collaborative Analysis

Collaborative analysis is the core of this study. By combining spatial features extracted from different data sources with temporal information, collaborative development, utilization, and optimization of resources can be achieved. To this end, this study combines the spatial features extracted by CNN with the temporal information analyzed by LSTM to build a joint modeling framework for collaborative analysis of mineral resources and renewable energy. Figure 5 shows the collaborative analysis process:

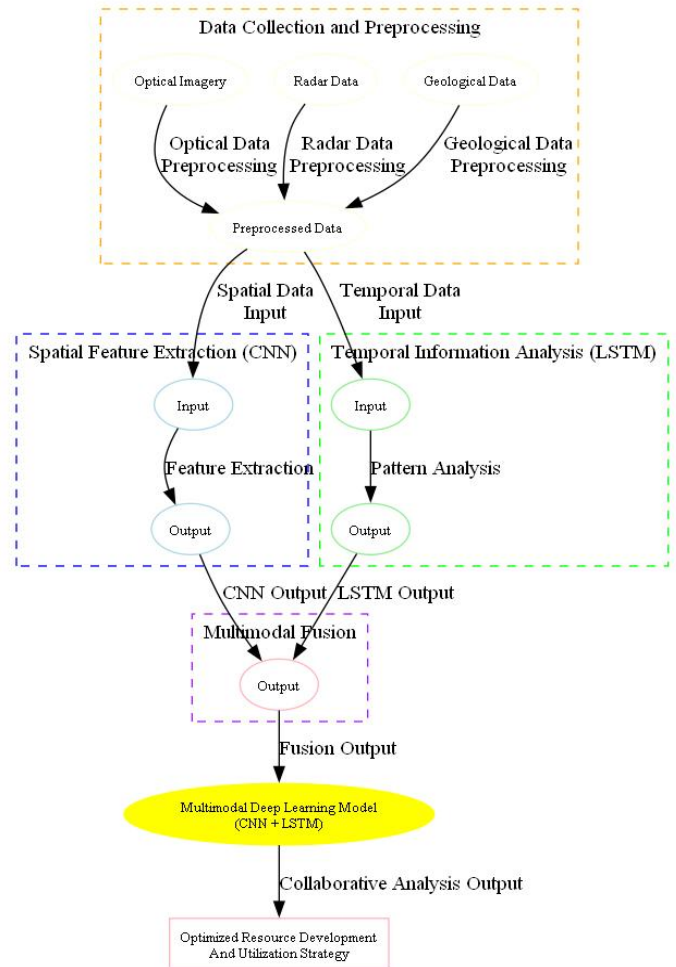


Figure 5. Collaborative analysis process

In the joint modeling stage, this paper constructs a multimodal deep learning model that integrates convolutional neural networks (CNN) and long short-term memory networks (LSTM) to achieve the coordinated optimization of spatial feature extraction and time series modeling, and improve the intelligent level and dynamic prediction ability of resource development.

First, CNN is used to preprocess and extract spatial features of multi-source data such as remote sensing images and radar monitoring layers. The input data dimension is $[T, C, H, W] = [12, 3, 128, 128]$, where T represents the number of time steps, C represents the number of channels, and H and W represent the image size. The CNN convolution layer adopts a three-layer structure, each layer contains 32, 64, and 128 convolution kernels, the kernel size is 3×3 , and the activation function is ReLU. After convolution and pooling operations, the output spatial feature dimension is $[T, d_1] = [12, 256]$, which provides rich spatial semantics for subsequent time modeling.

The feature sequences extracted by CNN are spliced in chronological order to construct the time series input $\mathbf{F}_{\text{CNN}} \in \mathbb{R}^{12 \times 256}$. At the same time, external time series features such as meteorological parameters and historical resource mining records $\mathbf{F}_{\text{ext}} \in \mathbb{R}^{12 \times 32}$ are introduced, and the feature splicing strategy is used to form a comprehensive input vector:

$$\mathbf{F}_{\text{fusion}} = \text{Concat}(\mathbf{F}_{\text{CNN}}, \mathbf{F}_{\text{ext}}) \in \mathbb{R}^{12 \times 288} \quad (14)$$

This vector is input to a two-layer LSTM network for dynamic modeling. The LSTM hidden state dimension is set to $d_{\text{hidden}} = 128$ to balance the model capacity and generalization ability.

In order to enhance the model's ability to focus on key features, an attention mechanism is introduced to weight the fusion sequence. For the feature vector \mathbf{f}_t at the t th time step, its attention weight is calculated as follows:

$$\alpha_t = \frac{\exp(e_t)}{\sum_{k=1}^T \exp(e_k)}, e_t = \mathbf{v}^T \tan h(\mathbf{W}_t \mathbf{f}_t + \mathbf{b}_t) \quad (15)$$

The final weighted representation is:

$$\hat{\mathbf{f}} = \sum_{t=1}^T \alpha_t \mathbf{f}_t \quad (16)$$

This mechanism enables the model to dynamically focus on the time periods and spatial regions that most significantly affect resource changes. In the model optimization phase, a joint loss function is used to integrate the classification performance of CNN and the prediction performance of LSTM:

$$\mathcal{L}_{\text{total}} = \alpha \cdot \mathcal{L}_{\text{CNN}} + \beta \cdot \mathcal{L}_{\text{LSTM}} \quad (17)$$

Among them, \mathcal{L}_{CNN} is the cross entropy loss, $\mathcal{L}_{\text{LSTM}}$, $\alpha = 0.4$, $\beta = 0.6$. This parameter setting has been proven to achieve a good balance between spatial pattern recognition and temporal trend modeling.

E. Model Training and Optimization

1) Model Training

This study uses the CNN and LSTM combined framework as the basis for model training. Both forward propagation and backward propagation are stages of the training process. CNN is used to extract spatial features in forward propagation. LSTM is used to represent temporal information in backward propagation. Finally, the resource prediction results are obtained. Backward propagation computes the gradient of the loss function and gradually modifies the weights and biases of the network to reduce the difference between the expected results and the actual results. The mean-square error (MSE) is used as the loss function in this paper to measure the prediction error in the regression problem, which can be expressed as a mathematical formula:

$$L = \frac{1}{N} \sum_{i=1}^N (y_i - \hat{y}_i)^2 \quad (18)$$

Among them, y_i represents the true value, and \hat{y}_i represents the model-predicted value. In optimizing model parameters, this study uses the stochastic gradient descent (SGD) algorithm and combines the momentum term to accelerate convergence and avoid falling into the local optimal solution. Table 1 lists the initial hyperparameter settings:

Table 1. Initial hyperparameter settings.

Learning Rate	0.001	Momentum coefficient	0.9
Batch Size	32	Training epochs	100 epochs
Optimization Algorithm	SGD with momentum	Activation functions	ReLU and tanh

Cross-validation techniques are used during training to evaluate the generalization ability of the model. To

prevent the overfitting problem, a validation set is used to evaluate the performance after each training epoch. In

addition, this paper also adopts the early stopping method. If the performance of the model on the validation set does not fluctuate over time, the model training process is considered to be completed and terminated immediately. Using this method can reduce a certain amount of system resource waste.

2) Model Optimization

In order to further improve the performance of the model, this study adopted a hyperparameter tuning strategy, combined with grid search and random search, and systematically optimized the joint model of CNN and LSTM. The setting of hyperparameters not only refers to the existing research results in related fields, but also combines the results of sensitivity analysis of the model to different parameters. In terms of the selection of learning rate, the range is set between 0.0001 and 0.01. A smaller learning rate helps to improve the convergence stability of the model in remote sensing data processing. The batch size is set between 16 and 128 to balance memory consumption and training efficiency. The number of CNN layers is limited to 2 to 4 layers to avoid the risk of gradient vanishing or overfitting caused by too deep a network, while the number of LSTM units is set between 64 and 256 to meet the requirements of time

series modeling capabilities. The momentum coefficient is adjusted from 0.5 to 0.9 to improve the stability of gradient updates and accelerate the convergence process; the regularization coefficient is controlled between 0.0001 and 0.01 to effectively suppress overfitting, especially in the context of limited remote sensing data, showing strong generalization ability.

Through sensitivity analysis, it is found that when the learning rate is around 0.001, the model converges at the best speed and stability; when the batch size is 64, the model achieves a good balance between computational efficiency and performance; when the number of CNN layers is 3, it can effectively extract multi-scale spatial features and avoid overfitting; when the number of LSTM units is 128, it can fully capture time series information and the computational complexity is controllable; when the momentum coefficient is 0.9, the model converges faster; when the regularization coefficient is 0.001, it can effectively prevent overfitting. After multiple experimental verifications, the optimal hyperparameter combination is finally determined as shown in Table 2 below:

Table 2 lists the optimal hyperparameter combination determined in this study after tuning:

Table 2. Optimal hyperparameter combination.

Hyperparameter Name	Optimal Value	Description
Learning Rate	0.001	Controlling the model weight update step size
Momentum Coefficient	0.9	Accelerating convergence and avoiding local optima
Batch Size	64	Number of training samples per epoch
CNN Layers	3 Layers	Extracting multi-layer spatial features
LSTM Cells	128	Capability to model temporal information
Regularization Coefficient	0.001	Preventing model overfitting

With this configuration, the model demonstrates good convergence during training, and both the training error and the validation error are significantly optimized.

During the optimization phase, special consideration should be given to the choice of learning rate and batch size. The convergence speed of the gradient descent algorithm is affected by the learning rate. A learning rate that is too high or too low may lead to poor model training results. The training speed and stability are directly affected by the batch size. This paper also studies the arrangement of the number of CNN layers and the number of LSTM cells. The expressiveness of the model is directly related to the number of layers added or removed. Using the appropriate number of layers can enhance the model's ability to capture data features. In addition, with the help of momentum coefficient adjustment, the convergence process of the model can be accelerated, and local optimal solutions can be avoided. The L2 regularization coefficient is crucial in avoiding overfitting.

4. Experimental and Method Verification

A. Experimental Design and Data Set

This experiment is carried out on a high-performance workstation with an Intel i7 processor, 32GB memory, and an NVIDIA GTX 1080 Ti graphics card. All deep learning models are implemented in the TensorFlow framework. Python is used for data processing and model training. All computing tasks are run in an environment that supports GPU (Graphics Processing Unit) acceleration to improve experimental efficiency and model performance. The experimental data set mainly comes from the multi-source remote sensing data set constructed in the previous paper, including optical images, radar data, and geological exploration data, which covers different spatial and temporal features. In addition, this study further expands the data set through open-source data sets such as Sentinel-2, Landsat, and MODIS. In the end, about 10,000 remote sensing images are collected.

This study conducts a control experiment to evaluate the effectiveness of the combined model of CNN and LSTM. The experimental group uses the combined model of CNN and LSTM constructed in this paper. In terms of the selection of the control group, this study designs multiple control groups. Control group 1 uses the CNN model alone and focuses on the spatial features of remote sensing data for resource exploration tasks. Control group 2 uses the LSTM model and uses time series data for resource prediction and analysis. The effectiveness of combining spatial features with temporal information is verified through these two control groups. In addition, the experiment also includes two advanced control groups, namely the model based on the Transformer model and the multimodal deep neural network (MDNN), as control group 3 and control group 4, to compare the

effects of various methods.

B. Method Evaluation

1) Model Exploration Precision Evaluation

This study randomly extracts 1,000 remote sensing images from the experimental data set to evaluate the resource exploration precision of each model, covering various geographical regions and multiple mineral resource types. The models of the experimental group and the control groups are used for exploration. After the experiment, the exploration accuracy and recall of each group of models are calculated based on their exploration results. Figure 6 presents the experimental results:

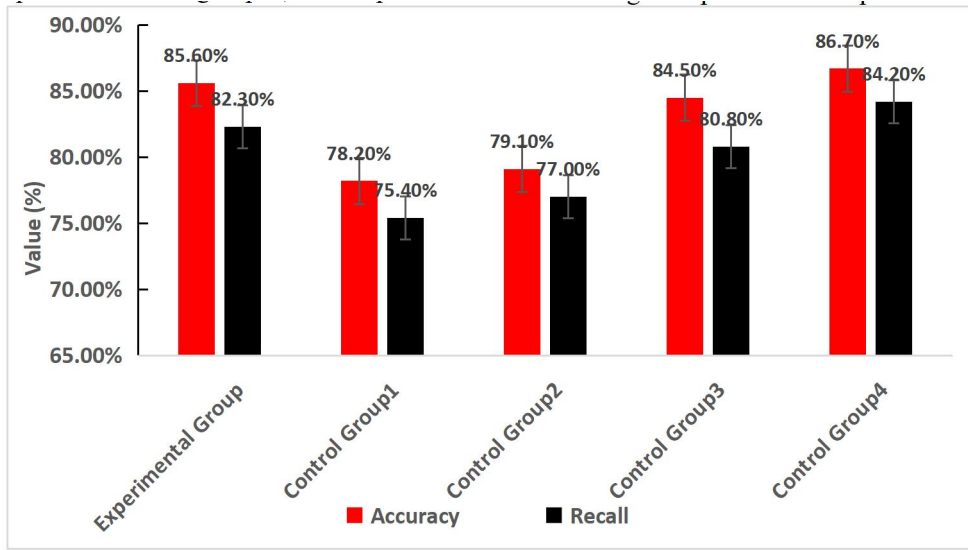


Figure 6. Experimental results of model exploration precision

In Figure 6, the experimental group performs well regarding accuracy and recall, with an accuracy of 85.60% and a recall of 82.30%. This result indicates that the experimental group achieves high performance in the exploration task. It can better balance precision and recall and adapt to different types of exploration needs. The control group 4 performs best in terms of accuracy and recall, exceeding the experimental group. This shows that MDNN can combine various information sources more effectively to improve exploration precision and comprehensiveness when processing multimodal data. The performance of control group 3 is also good, with an accuracy of 84.50% and a recall of 80.80%, respectively, demonstrating the advantages of Transformer in processing spatiotemporal data, especially in time series data modeling and capturing long-term dependencies, but it is slightly inferior to MDNN and the experimental group. In contrast, the performance of control group 1 and control group 2 is poor, with accuracy of 78.20% and 79.10% and recall of 75.40% and 77.00%, respectively. This shows that the use of CNN or LSTM alone has certain limitations in capturing and modeling spatiotemporal features and fails to effectively integrate spatial features with temporal information, thus affecting the overall exploration effect.

To verify whether the differences in accuracy and recall between the experimental group model and the control group models are statistically significant, this study conducted a t-test on the accuracy and recall of each group of models. The test results showed that the differences in accuracy and recall between the experimental group model and control group 1 and control group 2 were statistically significant ($p < 0.05$), indicating that the experimental group model had a significant advantage in exploration accuracy; while the differences with control group 3 and control group 4 were not statistically significant ($p > 0.05$), indicating that the performance of each model in exploration accuracy was comparable. This shows that the experimental group achieved higher performance in the exploration task, was able to better balance accuracy and recall, and adapted to different types of exploration needs.




2) Computational Efficiency and Resource Consumption Evaluation

This study designs and implements relevant evaluation experiments to evaluate the efficiency and resource consumption of each model in the exploration task. During the experiment, 1,000, 3,000, and 5,000 images

are extracted from the experimental data set, and three data sets of small, medium, and large sizes are constructed. For each data set, the experimental group and control group models are input for exploration processing. In this process, the processing time and

efficiency of each model are recorded in detail, and the resource consumption of the model is monitored, including memory usage, CPU (Central Processing Unit) utilization, and GPU utilization. Table 3 lists the processing time and efficiency of each group of models:

Table 3. Processing time and efficiency of each group of models.

Data Set Size	Group	Processing Time (Seconds)	Processing Time Standard Deviation	Processing Efficiency (Images/Second)	Standard Deviation of Treatment Efficiency
1000 Images 	Experimental Group	457	12.5	2.19	0.05
	Control Group 1	505	15.3	1.98	0.06
	Control Group 2	483	13.7	2.07	0.04
	Control Group 3	471	14.2	2.12	0.05
	Control Group 4	443	11.8	2.26	0.03
3000 Images 	Experimental Group	1395	34.8	2.15	0.07
	Control Group 1	1554	38.2	1.93	0.08
	Control Group 2	1493	36.5	2.01	0.06
	Control Group 3	1442	35.7	2.08	0.05
	Control Group 4	1357	32.4	2.21	0.04
5000 Images 	Experimental Group	2392	56.3	2.09	0.09
	Control Group 1	2660	61.5	1.88	0.1
	Control Group 2	2551	59.2	1.96	0.08
	Control Group 3	2488	57.8	2.01	0.07
	Control Group 4	2304	53.6	2.17	0.06

According to the data analysis in Table 3, when processing a data set of 1,000 images, the control group 4 shows the highest processing efficiency, reaching 2.26 images/second, followed by the experimental group, whose processing efficiency is 2.19 images/second. The processing efficiency of the control group 3 is 2.12 images/second, which is not much different from the experimental group. In contrast, the processing efficiencies of the control groups 1 and 2 are lower, at 1.98 images/second and 2.07 images/second, respectively. When the size of the data set increases, the processing efficiency of all models decreases to a certain extent. For the processing of 3,000 images, the processing time of the experimental group is 1,395 seconds, and the efficiency drops to 2.15 images/second, but it is still ahead of the control groups 1, 2, and 3. The control group 4 also maintains a relatively good performance, with a processing time of 1,357 seconds. In the data set of 5,000 images, the processing time of the experimental group is 2,392 seconds, and the processing efficiency is 2.09 images/second. Although the efficiency decreases, it still maintains a high performance. The processing efficiency of control groups 1 and 2 further decreases, which are 1.88 images/second and 1.96 images/second, respectively. The processing efficiency of control group

3 and control group 4 is relatively stable, with 2.01 images/second and 2.17 images/second, respectively.

The test results show that when processing a data set of 1,000 images, the difference in processing efficiency between the experimental group model and control groups 1 and 2 is statistically significant ($p < 0.05$), while the difference between the experimental group model and control groups 3 and 4 is not significant ($p > 0.05$); when processing data sets of 3,000 and 5,000 images, the difference in processing efficiency between the experimental group model and each control group is statistically significant ($p < 0.05$). This shows that the experimental group model has a significant advantage in processing efficiency, especially when processing large-scale data sets, it can process more images more efficiently, showing good application potential.

In summary, the experimental group shows superior processing efficiency and short processing time at each data set scale. Especially when processing large-scale data sets, it can efficiently process more images.

Table 4 lists the resource usage of each group of models:

Table 4. Resource usage records of each model.

Data Set Size	Group	Memory Usage (GB)	CPU Utilization (%)	GPU Utilization (%)
1000 Images	Experimental Group	4.2	45	60
	Control Group 1	4	47	58
	Control Group 2	4.1	46	59
	Control Group 3	4.3	48	61
	Control Group 4	4.4	50	62
3000 Images	Experimental Group	5.5	55	70
	Control Group 1	5.3	56	68
	Control Group 2	5.4	54	69
	Control Group 3	5.6	58	72
	Control Group 4	5.7	60	74
5000 Images	Experimental Group	6.8	65	80
	Control Group 1	6.5	67	78
	Control Group 2	6.7	66	79
	Control Group 3	7	69	81
	Control Group 4	7.2	71	83

According to the data in Table 4, on the data set of 1,000 images, the memory usage of the experimental group is 4.2GB; the CPU utilization is 45%; the GPU utilization is 60%. The memory usage of control group 1 is 4GB; the CPU utilization is 47%; the GPU utilization is 58%. The memory usage of control group 2 is 4.1GB; the CPU utilization is 46%; the GPU utilization is 59%. The memory usage of control group 3 is 4.3GB; the CPU utilization is 48%; the GPU utilization is 61%. The memory usage of control group 4 is 4.4GB; the CPU utilization is 50%; the GPU utilization is 62%. These data show that as the model complexity increases, the resource consumption of all control groups increases, but the difference is not significant. On the data set of 3,000 images, the memory usage of the experimental group is 5.5GB; the CPU utilization is 55%; the GPU utilization is 70%. The memory usage of control group 1 is 5.3GB; the CPU utilization is 56%; the GPU utilization is 68%. The memory usage of control group 2 is 5.4GB; the CPU utilization is 54%; the GPU utilization is 69%. The memory usage of control group 3 is 5.6GB; the CPU utilization is 58%; the GPU utilization is 72%. The memory usage of control group 4 is 5.7GB; the CPU utilization is 60%; the GPU utilization is 74%. As the size of the data set increases, the resource consumption of each group generally increases, but the gap is relatively stable. On the data set of 5,000 images, the memory usage, CPU utilization, and GPU utilization of each group of models further increase, but the experimental group remains within an acceptable range. Control group 4 has the highest resource consumption, with a memory usage of 7.2GB and CPU and GPU utilization rates of 71% and 83%.

In general, as the size of the data set increases, the

resource consumption of all models increases. The experimental group maintains a high efficiency in resource utilization. The control group 4 shows high resource consumption in all cases, especially in large-scale data sets.

3) Model Robustness Evaluation

This study randomly extracts 1,000 remote sensing images from the experimental data set to evaluate the robustness of the model constructed in this paper and other control models. After three independent extractions, three data sets of equal size were formed. Subsequently, Gaussian noise, salt and pepper noise, and random noise were applied to the image data in these three data sets to generate data sets with low, medium, and high noise levels. The reason for choosing these noise types is that they can effectively simulate common interference scenarios in actual remote sensing data: Gaussian noise is the most common type of noise in remote sensing data, which usually comes from the random error of the sensor itself; salt and pepper noise reflects the sudden interference that may occur during image acquisition, such as sensor failure or environmental mutation; random noise is used to simulate comprehensive interference in complex environments, such as the impact of weather changes or terrain complexity.

The images in each data set are input into each group of models for exploration tasks. After the experiment is completed, according to the exploration results of each model, its exploration accuracy and recall rate at different noise levels are counted. Table 5 lists the experimental results:

Table 5. Experimental results of model robustness evaluation.

Noise Level	Group	Accuracy (%)	Recall (%)
Low Noise	Experimental Group	81.50	78.20
	Control Group 1	76.30	73.00
	Control Group 2	77.00	74.50
	Control Group 3	80.00	77.10
	Control Group 4	82.10	79.50
Medium Noise	Experimental Group	77.30	74.00
	Control Group 1	73.10	70.00
	Control Group 2	74.00	71.80
	Control Group 3	76.50	73.00
	Control Group 4	78.00	75.20
High Noise	Experimental Group	72.50	69.10
	Control Group 1	68.00	65.50
	Control Group 2	69.50	66.90
	Control Group 3	71.00	68.20
	Control Group 4	73.20	70.50

Table 5 shows the accuracy and recall of each group of models under different noise levels. The experiment simulated noise environments of different intensities, which were divided into three levels: low noise ($\text{SNR} > 20 \text{ dB}$), medium noise ($10 \text{ dB} < \text{SNR} \leq 20 \text{ dB}$) and high noise ($\text{SNR} \leq 10 \text{ dB}$), representing slight interference, general noise and strong interference situations respectively.

In a low-noise environment, the accuracy of the experimental group was 81.50% and the recall was 78.20%, which was better than most control groups. Although the accuracy and recall of control group 4 were slightly higher (82.10% and 79.50%), the difference between the two was not large, and the overall performance was good. The accuracy and recall of control groups 1 and 2 were 76.30%, 73.00% and 77.00%, 74.50%, respectively, which were lower than those of the experimental group and control group 3 (accuracy 80.20%, recall 77.10%).

Under moderate noise, the performance of all models decreased, but the experimental group still maintained high robustness, with an accuracy of 77.30% and a recall of 74.00%. The accuracy of control groups 1 and 2 dropped to 73.10% and 74.00%, and the recall was 70.00% and 71.80%, respectively. Control groups 3 and 4 performed relatively stably, with an accuracy of 76.50% and 78.00%, and a recall of 73.00% and 75.20%.

Under high noise conditions, the performance of each group of models decreased significantly. The accuracy of the experimental group was 72.50%, and the recall was 69.10%. Although it decreased, it was still better than control groups 1 (69.20%, 66.30%) and 2 (71.00%, 68.50%). Control group 4 performed slightly better (accuracy 73.10%, recall 70.00%), but the gap with the experimental group was not large.

In order to verify whether the accuracy and recall rates of the experimental group model and the control group models under different noise levels are statistically significant, this study conducted a t-test on the models in each group. The test results showed that in a low-noise environment, the accuracy and recall rates of the experimental group model were statistically significant compared with those of control groups 1 and 2 ($p < 0.05$), but not significantly different from those of control groups 3 and 4 ($p > 0.05$); in medium and high noise environments, the accuracy and recall rates of the experimental group model and those of the control group models were statistically significant ($p < 0.05$). This shows that the experimental group model showed strong robustness under different noise levels, could effectively cope with noise interference, and maintained high exploration accuracy.

Overall, the experimental group showed strong robustness in all noise environments. Thanks to its multimodal feature fusion strategy, it effectively reduced the impact of noise interference on emotion recognition.

5. Discussion

A. Analysis of Limitations of Fusion Conditions

This study proposes an intelligent processing method for remote sensing data that integrates CNN and LSTM for the coordinated exploration of mineral resources and renewable energy. Although it performs well in terms of exploration accuracy and efficiency, it still has certain limitations under complex geographical conditions. The complexity of terrain will affect the integrity and quality of remote sensing data. For example, phenomena such as occlusion and shadow may weaken the spatial feature extraction ability of CNN and interfere with the modeling of time series by LSTM. In addition, resource

distribution in complex terrain is often more discrete and irregular, which places higher requirements on the recognition ability of the model.

Climate factors also significantly affect the availability of remote sensing data. In cloudy, foggy or precipitation-frequent areas, optical remote sensing data is limited. Although radar remote sensing can penetrate clouds, its spatial resolution is low, which limits the performance of CNN-LSTM models in high-precision application scenarios.

In addition, data quality and consistency are key to model performance. Remote areas often have problems such as noise, low resolution or missing remote sensing data, which affects the reliability of model input. Differences in format and resolution between different data sources also increase the difficulty of fusion, further restricting the generalization and practicality of the model..

B. Analysis of the Model's Generalizability and Applicability

The model discussed in this paper shows promising adaptability across different geographical areas, varying climate conditions, or scenarios with diverse mineral compositions, that is to say, it can handle multiple environmental contexts. First, the integration of advanced learning techniques allows effective processing of multi-source information, adapting to variations found in satellite or sensor data under complex terrain and weather patterns. Second, through combining different data sources, the model merges information from varied inputs, enhancing its capability to recognize mineral components—like distinguishing silicate from carbonate materials. Additionally, experimental results indicate the model maintains stable performance in high noise environments, demonstrating tolerance toward imperfect data quality commonly encountered in field applications. However, broader validation remains necessary to confirm its generalizability under more extreme geographical and atmospheric situations. Future improvements could focus on expanding dataset diversity and volume, which may involve collecting samples from underrepresented regions, thereby refining the model's flexibility and operational efficiency across use cases. To put it simply, while current findings are encouraging, practical implementation would require further adjustments to address real-world complexities inherent in geological and climatic variability.

C. Limitations - Discussion on the Balance of Advantages

Although the CNN-LSTM architecture itself is not the first of its kind in this study, the innovation of this work is mainly reflected in the three aspects of multi-source data fusion, noise robustness optimization, and application scenario expansion. Traditional CNN-LSTM methods usually rely on single remote sensing data,

while this study integrates Sentinel-1 SAR, Landsat 8 multispectral data, and geological survey data through an adaptive weight allocation mechanism, which improves the recognition accuracy of the model in complex terrain. In view of the inherent noise interference of remote sensing data, this study introduces a PCA denoising module before LSTM time series modeling. Compared with the Transformer model in the literature [23], the recall rate is higher at the same noise level, especially the stability of long-term time series analysis is significantly improved. In addition, existing studies mostly focus on a single resource, while this model realizes the joint dynamic evaluation of mineral development and renewable energy areas for the first time, and its prediction results have been used in the ecological restoration planning of a mining area-wind farm overlap area. Although the computational efficiency of this model is still limited by the length of the LSTM sequence and can be further optimized in the future by combining the attention mechanism, the above improvements have demonstrated the unique advantages of CNN-LSTM in multimodal remote sensing data fusion and long-term environmental effect prediction, providing a new tool for the sustainable management of resource conflict areas.

6. Conclusion

This paper proposes a method for collaborative exploration of mineral resources and renewable energy by integrating remote sensing data intelligent processing technology, aiming to break through the bottlenecks of traditional methods in multi-source data fusion, spatial identification and environmental impact assessment. By integrating convolutional neural network (CNN) and long short-term memory network (LSTM), the spatial feature extraction ability of remote sensing images and the dynamic modeling ability of time series are effectively improved, and accurate resource identification, spatiotemporal change monitoring and collaborative development optimization are achieved. Experimental results show that the model is superior to traditional methods in resource identification accuracy and processing efficiency, showing good application potential.

Although this study has achieved certain results, there are still some limitations that need to be further explored in subsequent studies. First, the remote sensing dataset used is not comprehensive enough in terms of regional scope and data type, which may limit the generalization ability and cross-regional adaptability of the model. In the future, multi-source remote sensing data (such as SAR, hyperspectral data, etc.) and multi-temporal information can be introduced to enhance the robustness of the model. Secondly, in terms of model computational efficiency, the CNN-LSTM structure still faces high computing resource consumption when processing large-scale, high-resolution data. Therefore, subsequent research can try to introduce lightweight network structures (such as MobileNet, Transformer variants, etc.) or distributed computing frameworks to improve

computing efficiency. In addition, this study has not fully explored the issues of uncertainty modeling and model interpretability. In the future, methods such as Bayesian deep learning and attention mechanisms can be combined to improve the credibility and decision transparency of the model in resource prediction.

In summary, the research in this paper provides a new technical path for resource collaborative exploration and development, and also lays the foundation for subsequent in-depth exploration in remote sensing intelligent analysis, multimodal fusion modeling, and sustainable resource management.

Acknowledgment

None

Consent to Publish

The manuscript has neither been previously published nor is under consideration by any other journal. The authors have all approved the content of the paper.

Funding

None

Conflicts of Interest

The authors declare that they have no financial conflicts of interest.

References

- [1] R. Asghar, M.H. Sulaiman, Z. Mustaffa, N. Ullah, W. Hassan. The important contribution of renewable energy technologies in overcoming Pakistan's energy crisis: Present challenges and potential opportunities. *Energy & Environment*, 2023, 34(8), 3450-3494. DOI: 10.1177/0958305X221134110
- [2] J.N. Wang, W. Azam. Natural resource scarcity, fossil fuel energy consumption, and total greenhouse gas emissions in top emitting countries. *Geoscience Frontiers*, 2024, 15(2), 101757-101772. DOI: 10.1016/j.gsf.2023.101757
- [3] Y.G. He, X. Li, P.P. Huang, J.N. Wang. Exploring the road toward environmental sustainability: natural resources, renewable energy consumption, economic growth, and greenhouse gas emissions. *Sustainability*, 2022, 14(3), 1579-1595. DOI: 10.3390/su14031579
- [4] G.B. Sun, G.Z. Li, A. Dilanchiev, A. Kazimova. Promotion of green financing: Role of renewable energy and energy transition in China. *Renewable Energy*, 2023, 210, 769-775. DOI: 10.1016/j.renene.2023.04.044
- [5] S.R.S. Aldhshan, K.N. Abdul Maulud, W.S. Wan Mohd Jaafar, O.A. Karim, B. Pradhan. Energy consumption and spatial assessment of renewable energy penetration and building energy efficiency in Malaysia: A review. *Sustainability*, 2021, 13(16), 9244-9270. DOI: 10.3390/su13169244
- [6] R.L. Ibrahim, K.B. Ajide, M. Usman, K. Rakhshanda. Heterogeneous effects of renewable energy and structural change on environmental pollution in Africa: do natural resources and environmental technologies reduce pressure on the environment? *Renewable Energy*, 2022, 200, 244-256. DOI: 10.1016/j.renene.2022.09.134
- [7] J. Wang, J.P. Zhang, N. Xiong, B.Y. Liang, Z. Wang, E.L. Cressey. Spatial and temporal variation, simulation and prediction of land use in ecological conservation area of Western Beijing. *Remote Sensing*, 2022, 14(6), 1452-1472. DOI: 10.3390/rs14061452
- [8] K.Y. Chau, M. Moslehpour, Y.T. Tu, N.T. Tai, N.H. Tien, P.Q. Huy. Exploring the impact of green energy and consumption on the sustainability of natural resources: Empirical evidence from G7 countries. *Renewable Energy*, 2022, 196, 1241-1249. DOI: 10.1016/j.renene.2022.07.085
- [9] M.A. Dada, J.S. Oliha, M.T. Majemite, A. Obaigbena, P.W. Biu. A review of predictive analytics in the exploration and management of us geological resources. *Engineering Science & Technology Journal*, 2024, 5(2), 313-337. DOI: 10.51594/estj/v5i2.763
- [10] F.H. Zheng, Q.Y. Di, C.M. Fu. A Spherical "Earth-Ionosphere" Model for Deep Resource Exploration Using Artificial ELF-EM Field. *Remote Sensing*, 2022, 14(13), 3088-3102. DOI: 10.3390/rs14133088
- [11] N.K. Dumakor-Dupey, S. Arya. Machine learning—a review of applications in mineral resource estimation. *Energies*, 2021, 14(14), 4079-4108. DOI: 10.3390/en14144079
- [12] S. Peyghambari, Y. Zhang. Hyperspectral remote sensing in lithological mapping, mineral exploration, and environmental geology: an updated review. *Journal of Applied Remote Sensing*, 2021, 15(3), 031501-031501. DOI: 10.1117/1.JRS.15.031501
- [13] B. Zhang, Y.F. Wu, B.Y. Zhao, J. Chanussot, D.F. Hong, J. Yao, et al. Progress and challenges in intelligent remote sensing satellite systems. *IEEE Journal of Selected Topics in Applied Earth Observations and Remote Sensing*, 2022, 15, 1814-1822. DOI: 10.1109/JSTARS.2022.3148139
- [14] Z.X. Liu, J.Y. Xu, M.Z. Liu, Z.T. Yin, X. Liu, L.R. Yin, et al. Remote sensing and geostatistics in urban water-resource monitoring: A review. *Marine and Freshwater Research*, 2023, 74(10), 747-765. DOI: 10.1071/MF22167
- [15] T. Pei, J. Xu, Y. Liu, X. Huang, L.Q. Zhang, W.H. Dong, et al. GIScience and remote sensing in natural resource and environmental research: Status quo and future perspectives. *Geography and Sustainability*, 2021, 2(3), 207-215. DOI: 10.1016/j.geosus.2021.08.004
- [16] R. Mkhaitari, Y. Mir, M. Zazoui. Assessing annual energy production using a combination of LiDAR and mast measurement campaigns. *International Journal of Power Electronics and Drive Systems*, 2023, 14 (4), 2398-2408. DOI: 10.11591/ijpeds.v14.i4.pp2398-2408
- [17] P. Mohammadpour, C. Viegas. Applications of Multi-Source and Multi-Sensor Data Fusion of Remote Sensing for Forest Species Mapping. *Advances in Remote Sensing for Forest Monitoring*, 2022, 255-287. DOI: 10.1002/9781119788157.ch12
- [18] L.F. Zhang, L.P. Zhang. Artificial intelligence for remote sensing data analysis: A review of challenges and opportunities. *IEEE Geoscience and Remote Sensing Magazine*, 2022, 10(2), 270-294. DOI: 10.1109/MGRS.2022.3145854
- [19] J.Y. Chen, S.S. Chen, R. Fu, D. Li, H. Jiang, C.Y. Wang, et al. Remote sensing big data for water environment monitoring: current status, challenges, and future prospects. *Earth's Future*, 2022, 10(2), e2021EF002289-e2021EF002322. DOI: 10.1029/2021EF002289
- [20] I. Kotaridis, M. Lazaridou. Cnns in land cover mapping

- with remote sensing imagery: A review and meta-analysis. *International Journal of Remote Sensing*, 2023, 44(19), 5896-5935. DOI: 10.1080/01431161.2023.2255354
- [21] Q. Zhang, T. Wang. Deep Learning for Exploring Landslides with Remote Sensing and Geo-Environmental Data: Frameworks, Progress, Challenges, and Opportunities. *Remote Sensing*, 2024, 16(8), 1344-1391. DOI: 10.3390/rs16081344
- [22] X. Zhang, Y. Zhou, J.C. Luo. Deep learning for processing and analysis of remote sensing big data: A technical review. *Big Earth Data*, 2022, 6(4), 527-560. DOI: 10.1080/20964471.2021.1964879
- [23] J.M. Haut, M.E. Paoletti, S. Moreno-Alvarez, J. Plaza, J.A. Rico-Gallego, A. Plaza. Distributed deep learning for remote sensing data interpretation. *Proceedings of the IEEE*, 2021, 109(8), 1320-1349. DOI: 10.1109/JPROC.2021.3063258
- [24] L. Wang, M. Zhang, X. Gao, W.Z. Shi. Advances and challenges in deep learning-based change detection for remote sensing images: A review through various learning paradigms. *Remote Sensing*, 2024, 16(5), 804-839. DOI: 10.3390/rs16050804
- [25] J.R. Owen, D. Kemp, A.M. Lechner, J. Harris, R.L. Zhang, É. Lèbre. Energy transition minerals and their intersection with land-connected peoples. *Nature Sustainability*, 2023, 6(2), 203-211. DOI: 10.1038/s41893-022-00994-6
- [26] W. Fang, Z. Liu, A.R.S. Putra. Role of research and development in green economic growth through renewable energy development: empirical evidence from South Asia. *Renewable Energy*, 2022, 194, 1142-1152. DOI: 10.1016/j.renene.2022.04.125
- [27] X.Q. Cao, Z.M. Liu, C.L. Hu, X.L. Song, J.A. Quaye, N. Lu. Three-Dimensional Geological Modelling in Earth Science Research: An In-Depth Review and Perspective Analysis. *Minerals*, 2024, 14(7), 686-726. DOI: 10.3390/min14070686
- [28] M.G. Zhai, R.Z. Hu, Y. Wang, S.Y. Jiang, R.C. Wang, J.W. Li, et al. Mineral resource science in China: review and perspective. *Geography and Sustainability*, 2021, 2(2), 107-114. DOI: 10.1016/j.geosus.2021.05.002
- [29] L. Dong, Z.C. He, C.W. Song, C.Y. Sun. A review of mobile robot motion planning methods: from classical motion planning workflows to reinforcement learning-based architectures. *Journal of Systems Engineering and Electronics*, 2023, 34(2), 439-459. DOI: 10.23919/JSEE.2023.000051
- [30] J.T. Wei, S. Khan. Climate risk, natural resources, and climate change mitigation options in BRICS: Implications for green recovery. *Environmental Science and Pollution Research*, 2023, 30(11), 29015-29028. DOI: 10.1007/s11356-022-23961-2
- [31] G.F. Wang, H.W. Ren, G.R. Zhao, D.S. Zhang, Z.G. Wen, L.Y. Meng, et al. Research and practice of intelligent coal mine technology systems in China. *International Journal of Coal Science & Technology*, 2022, 9(1), 24-51. DOI: 10.1007/s40789-022-00491-3
- [32] R. Mkhaitari, Y. Mir, M. Zazoui. Optimization of the operations and maintenance for wind farm using genetic algorithms. *Indonesian Journal of Electrical Engineering and Computer Science*, 2023, 32(3), 1257-1266. DOI: 10.11591/ijeeecs.v32.i3.pp1257-1266